

# Random nanolasing in the Anderson localized regime

J. Liu<sup>1,2,3</sup>, P. D. Garcia<sup>2</sup>, S. Ek<sup>1</sup>, N. Gregersen<sup>1</sup>, T. Suhr<sup>1</sup>, M. Schubert<sup>1†</sup>, J. Mørk<sup>1</sup>, S. Stobbe<sup>2</sup> and P. Lodahl<sup>2\*</sup>

**The development of nanoscale optical devices for classical and quantum photonics<sup>1–5</sup> is affected by unavoidable fabrication imperfections that often impose performance limitations. However, disorder may also enable new functionalities<sup>6</sup>, for example in random lasers, where lasing relies on random multiple scattering<sup>7–13</sup>. The applicability of random lasers has been limited due to multidirectional emission, lack of tunability, and strong mode competition<sup>11</sup> with chaotic fluctuations<sup>14</sup> due to a weak mode confinement. The regime of Anderson localization of light<sup>15</sup> has been proposed for obtaining stable multimode random lasing<sup>16</sup>, and initial work concerned macroscopic one-dimensional layered media<sup>17</sup>. Here, we demonstrate on-chip random nanolasers where the cavity feedback is provided by the intrinsic disorder. The strong confinement achieved by Anderson localization reduces the spatial overlap between lasing modes, thus preventing mode competition and improving stability. This enables highly efficient, stable and broadband wavelength-controlled lasers with very small mode volumes. Furthermore, the complex interplay between gain, dispersion-controlled slow light, and disorder is demonstrated experimentally for a non-conservative random medium. The statistical analysis shows a way towards optimizing random-lasing performance by reducing the localization length, a universal parameter.**

In a strongly scattering random medium, light can be trapped by concurrent multiple scattering events leading to the formation of localized cavity modes that prevail after averaging over all statistical configurations of disorder. Such Anderson localization is found to occur in state-of-the-art photonic-crystal waveguides where unavoidable intrinsic fabrication disorder is sufficient to induce localized cavities in the slow-light regime of waveguide propagation<sup>6</sup>. (For further details see Supplementary Section 1.) Adding gain to such a waveguide enables the study of the formation of the lasing modes that were attributed to disorder in previous work<sup>18</sup>. Figure 1a illustrates lasing cavities, which are spatially distributed along the waveguide and appear spectrally in the slow-light regime<sup>19</sup>. In the present experiment, quantum wells were embedded as a gain medium in the photonic-crystal membrane and were optically pumped. In a conservative one-dimensional single-mode waveguide, the Anderson localization criterion requires that the average distance between random scattering events, the localization length  $\xi$ , is shorter than the sample length  $L$ , and their ratio universally determines the confinement of the localized modes. The presence of absorption or gain changes this simple picture, because they will respectively damp or enhance the localized modes<sup>20</sup>, and may give rise to nonlinearities<sup>21</sup>. In the present experiment, for low

excitation pump power, the fluorescence emitted by the excited region of the quantum wells is multiply scattered along the waveguide, but is damped due to the strong absorption of the unpumped surrounding gain material, as shown in Fig. 1b. By increasing the excitation power, the light amplification compensates loss and the lasing threshold is reached. At the threshold, the system resembles a conservative waveguide. Here, we record a localization length that is more than ten times shorter than the sample length, thus confirming Anderson localization. Increasing the excitation power further leads to random lasing, as shown graphically in Fig. 1c. Figure 1d presents the emission spectrum of a single Anderson localized lasing mode below and above threshold, while Fig. 1e shows the peak output emission intensity versus input excitation power. A distinct lasing threshold is observed, accompanied by a decrease in the cavity linewidth with excitation power, both of which are signatures of laser oscillation. Two important figures of merit of a nanolaser are its  $\beta$ -factor (the fraction of spontaneous emission that couples to the lasing mode) and the cavity mode volume (the spatial extension of the lasing mode). These can be determined by modelling the laser input–output curves with microcavity semiconductor laser rate equations<sup>22</sup> (cf. Fig. 1e). The saturation observed at high excitation power is attributed to thermal effects (for details see Supplementary Section 4). For this particular lasing mode we obtain a  $\beta$ -factor of 0.31, which, interestingly, is significantly larger than previous values reported in photonic-crystal lasers with quantum-well gain media<sup>23</sup>. A mode volume of  $4.53(\lambda/n)^3$  is obtained, where  $\lambda = 1,587$  nm is the lasing wavelength and  $n = 3.4$  is the refractive index of InGaAsP, which is consistent with the mode extent found for Anderson localized modes in cavity quantum electrodynamics experiments in similar structures without the gain material<sup>24,25</sup>.

Determined by the size of the pumped area on the waveguide, multifrequency lasing can be observed (Fig. 1f,g). As shown in Fig. 1f, the onset of multimode lasing tends to be sequential; that is, with increasing excitation power the laser peaks grow one by one, each displaying the characteristic input–output lasing curve (Fig. 1g). A recent theoretical study predicted the strong suppression of interactions in multimode random lasing in the Anderson localization regime<sup>16</sup>. As shown in Fig. 1h, very stable lasing wavelengths are indeed observed, even for spectrally close lasing modes. This is attributed to the fact that the lasing modes overlap very weakly due to their (on average) exponential confinement<sup>16</sup>. In diffusive random lasers, in contrast, the extended lasing modes imply that different modes overlap spatially, inducing strong mode competition and chaotic lasing emission and therefore spectrally broad averaged emission<sup>14</sup>. In our case, the very narrow lasing linewidths

<sup>1</sup>DTU Fotonik, Department of Photonics Engineering, Technical University of Denmark, Ørsteds Plads 343, DK-2800 Kgs. Lyngby, Denmark, <sup>2</sup>Niels Bohr Institute, University of Copenhagen, Blegdamsvej 17, DK-2100 Copenhagen, Denmark, <sup>3</sup>South China Academy of Advanced Optoelectronics, South China Normal University, 510006 Guangzhou, China; <sup>†</sup>Present address: Universitt Konstanz, Fachbereich Physik, Fach M 700, 78457 Konstanz, Germany.

\*e-mail: lodahl@nbi.ku.dk

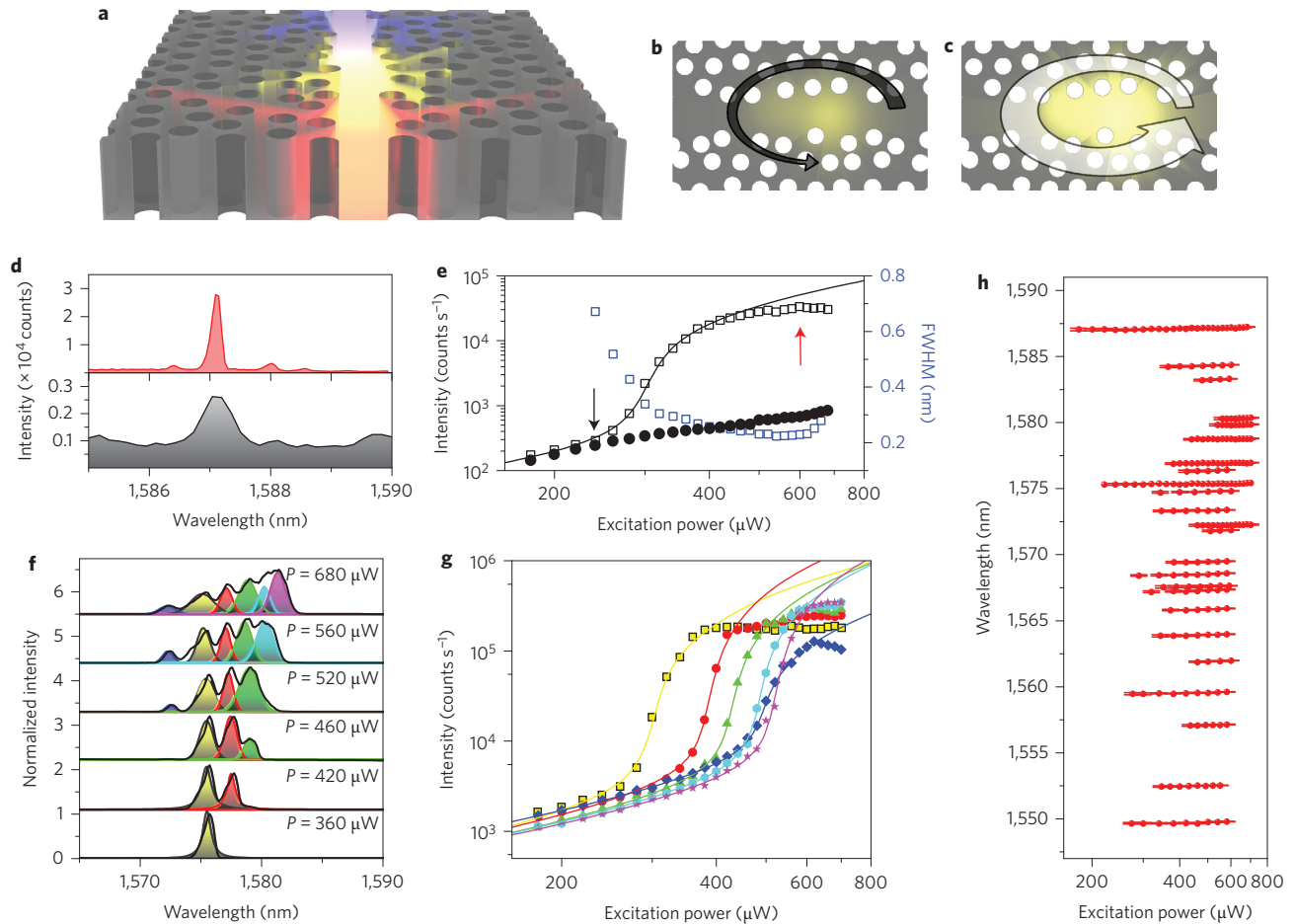


**Figure 1 | Single-mode and multimode random lasing in the Anderson localization regime.** **a**, Illustration of a random laser in a disordered photonic-crystal waveguide formed from Anderson localized modes, where the different colours indicate that multifrequency lasing can occur. **b, c**, Illustration of multiple-scattering process, where arrows represent optical feedback below (**b**) and above (**c**) threshold, respectively. Below threshold, loss dominates and Anderson localized cavities do not build up. Above threshold, gain compensates loss and Anderson localized random lasing sets in. **d**, Measured photoluminescence spectra of a single Anderson localized lasing mode below (black curve) and above (red curve) the lasing threshold under 240  $\mu\text{W}$  and 600  $\mu\text{W}$  excitation power, respectively. **e**, Output intensity (black squares) and linewidth (blue squares) measured versus excitation power (full width at half maximum, FWHM). The solid line represents a fit to semiconductor laser rate equations and black circles represent the background quantum-well fluorescence displaying no lasing. Black and red arrows indicate the excitation power of the spectra below and above the threshold shown in **d**. **f**, Photoluminescence spectra versus excitation power in multimode operation, where the different coloured curves are fits with Lorentzian functions representing different lasing modes. The curves are offset for clarity. **g**, Output intensity versus excitation power corresponding to the different lasing modes in **f**. Solid lines represent fits to semiconductor laser rate equations for each lasing mode. **h**, Central wavelength obtained from a Lorentzian fit of all the measured modes versus excitation power.

indicate the absence of chaotic operation. This linear non-interacting behaviour of lasing modes has been proposed as a tell-tale signal of Anderson localization in random lasing<sup>16</sup>.

In diffusive random lasers the lasing wavelength is primarily determined by the spectral peak of the gain medium<sup>7</sup>, while only weak dispersion is incorporated into the multiple-scattering medium, enabling modest tunability of the random laser<sup>10,26</sup>. A photonic-crystal waveguide, in contrast, is highly dispersive, which suggests that the Anderson localized random lasers can be spectrally shifted over an unprecedented wavelength range by varying the photonic-crystal lattice, with the only limitation given by the bandwidth of the quantum-well gain medium (almost 300 nm). Figure 2a demonstrates spectral control of the lasing modes over 50 nm when varying the ratio  $r/a$ , where  $r$  is the hole radius and  $a$  the lattice constant of the photonic-crystal waveguide. This broad wavelength control is due to a particular characteristic of Anderson localized modes in photonic-crystal waveguides: the modes appear solely in the slow-light regime of the waveguide near the band-edge cutoff, where the density of optical states (DOS) associated with the

waveguide mode is large<sup>27</sup>. Figure 2b shows how the high-DOS region of the waveguide can be controlled by varying the photonic-crystal parameters, establishing the wavelength-shifting mechanism for the Anderson localized modes.

A main goal of statistical physics is to establish general concepts and equations applying to macroscopic physical systems, despite differences in their microscopic details. Anderson localization is an example of such a concept; in essence it is a statistical phenomenon and therefore the statistics of the lasing parameters are the key quantities describing Anderson localization. The  $Q$ -factor distribution for all modes observed in the experiment, at lasing threshold, is shown in Fig. 3a, where the  $Q$ -factor is obtained as the ratio between the cavity centre wavelength and the cavity linewidth. From these data, the localization length and the loss length are obtained<sup>24</sup>. A localization length of  $\xi = 6.0 \mu\text{m}$  and loss length of  $l = 800 \mu\text{m}$  are extracted, with the latter determined by out-of-plane scattering and absorption in the unpumped region of the quantum well, which is likely to be biased towards low loss because, preferentially, the very localized modes will lase. At

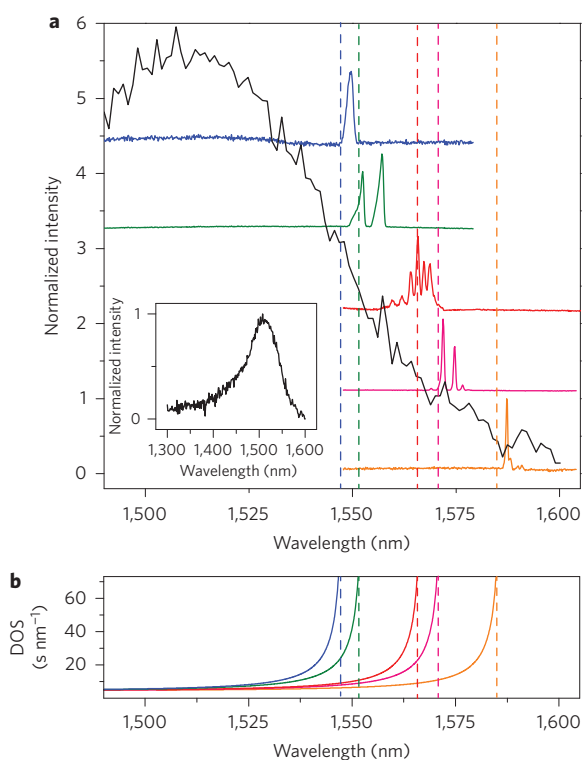


**Figure 2 | Controlling the Anderson localized random lasing wavelength.**

**a.** Photoluminescence spectra (shifted vertically for visual clarity) above lasing threshold collected for  $r/a = 0.237$  (orange curve), 0.243 (pink), 0.250 (red), 0.257 (green) and 0.263 (blue), where  $r$  is the hole radius and  $a$  the lattice constant of the photonic crystal. The black line plots the quantum-well emission spectrum for comparison (fully shown in the inset). **b.** Calculated DOS of a photonic-crystal waveguide without disorder where the different colours correspond to the different values of  $r/a$  in **a**. Vertical dashed lines indicate spectral positions of the slow-light regime where the DOS is large and lasing occurs.

threshold excitation power, light amplification compensates loss and the criterion for one-dimensional Anderson localization in a passive waveguide applies. Indeed, the obtained localization length is very similar to the value measured in photonic-crystal waveguides without gain<sup>24</sup>, and it is significantly shorter than the sample length of  $L = 100 \mu\text{m}$ , so the sample is found to be deeply in the Anderson localization regime. Figure 3b presents the distribution of lasing thresholds observed experimentally. An asymmetric threshold distribution with a long tail extending to high threshold values is obtained, as predicted by theory<sup>28</sup>, in contrast to the symmetric threshold distributions observed for diffusive random lasers<sup>29</sup>. The average threshold of  $418 \mu\text{W}$  is comparable to the typical threshold of standard photonic-crystal lasers pumped in a similar geometry<sup>23,30</sup> and is 20 times lower than the threshold measured for a macroscopically structured one-dimensional disordered medium in the localized regime<sup>17</sup>. The  $\beta$ -factor and mode-volume distributions are plotted in Fig. 3c,d, respectively. Large  $\beta$ -factors ranging from 0.28 to 0.38 are found for all lasing modes, in conjunction with small mode volumes ranging from 4 to  $6(\lambda/n)^3$ . The mode-volume distribution enables another estimate of the mode-length extension along the waveguide (see Supplementary Information), which is plotted as the top horizontal axis in Fig. 3d. The average mode length of  $4.3 \mu\text{m}$  is very similar to the localization length ( $\xi = 6.0 \mu\text{m}$ ) extracted by modelling the  $Q$ -factor distributions. This remarkable agreement confirms the validity of the two independent models applied to analyse the different experimental data, and illustrates that important microscopic

parameters of Anderson localized random lasers can be extracted reliably.

An interesting question is to what extent the performance of the Anderson localized random laser could be improved even further. Figure 3e,f and g,h show the measured lasing threshold and  $\beta$ -factor versus  $Q$ -factor and mode volume. The correlation between these parameters is quantified by the Spearman's rank correlation coefficient  $r_s$  (for details see Supplementary Section 6), which demonstrates how a high  $Q$ -factor and a small mode volume improve lasing performance. The key to improving these cavity characteristics of Anderson localized lasers even further would be to shorten the localization length. This may be feasible, for example, by combining random disorder with correlated order. Indeed, a shorter localization length could be beneficial in two ways, as it would increase the laser  $Q$ -factor while simultaneously decreasing the mode volume<sup>25</sup>. We note that the performance of the Anderson localized laser is not expected to be dependent solely on the universal parameter  $\xi/L$ , as this would determine only the propagation of light in the cavity; the emission of photons has been found to be non-universal, that is, dependent on the local dielectric topography of the sample. Such non-universality has been found to play a role in quantum optics effects on single quantum emitters<sup>31</sup> and is expected to have a minor effect in the broadband-emitter case of a random laser with quantum wells as the gain material (Supplementary Section 5). The current exploration of light emission and propagation in random media reveals the exciting prospects of disordered nanostructures for lasers and cavity quantum electrodynamics experiments.

Anderson localization was originally proposed for electronic transport where the total number of particles is conserved, but was later extended to non-conservative bosonic fields such as light. Any amount of absorption or light leakage from the structure reduces the confinement due to Anderson localization. Although the inclusion of large amounts of gain inevitably modifies the properties of the underlying ordered structure<sup>32</sup>, moderate optical gain can compensate the effect of loss, thereby recovering the confinement of light. The effect of gain on Anderson localization can be further investigated by extracting the probability distribution of the intensity fluctuations,  $P(\hat{I} \equiv I/\langle I \rangle)$ , where  $\langle I \rangle$  denotes the intensity obtained after ensemble averaging over configurations of disorder. The photoluminescence speckle pattern intensity  $I$  was measured while raster-scanning the sample, as shown in Fig. 4a (see Methods), and is displayed for different excitation powers in Fig. 4b. For low excitation power, the strong absorption from the quantum wells damps long interference paths, resulting in the normal distribution of  $P(\hat{I})$  shown in Fig. 4b. Increasing excitation power implies that gain compensates loss, and localized random lasing is observed. This behaviour can be qualitatively reproduced with a one-dimensional multiple scattering model<sup>24</sup> where the effect of gain is modelled by increasing the loss length (Fig. 4c). The experimentally recorded variance of the intensity fluctuations,  $\text{var}(\hat{I})$ , is found to increase monotonically with excitation power, as shown in Fig. 4d. The corresponding threshold for the variance of the intensity fluctuations for a passive sample that marks the onset of the Anderson localized regime is  $\text{var}(\hat{I}) = 1.37$  (Supplementary Section 3), which is surpassed at high pump powers. The relatively small intensity fluctuations observed here compared to passive samples<sup>6</sup> are attributed to the fact that in recording the statistics, some of the modes are below threshold and therefore damped, and only for parts of the modes is the loss compensated by gain. The ability to manipulate loss and gain in a one-dimensional random system opens the possibility of exploring the rich phase space of Anderson localization in bosonic systems, which has been studied only theoretically so far<sup>33</sup>. Controlling the interplay between gain and loss may offer exciting possibilities of fine-tuning the Anderson localized modes.

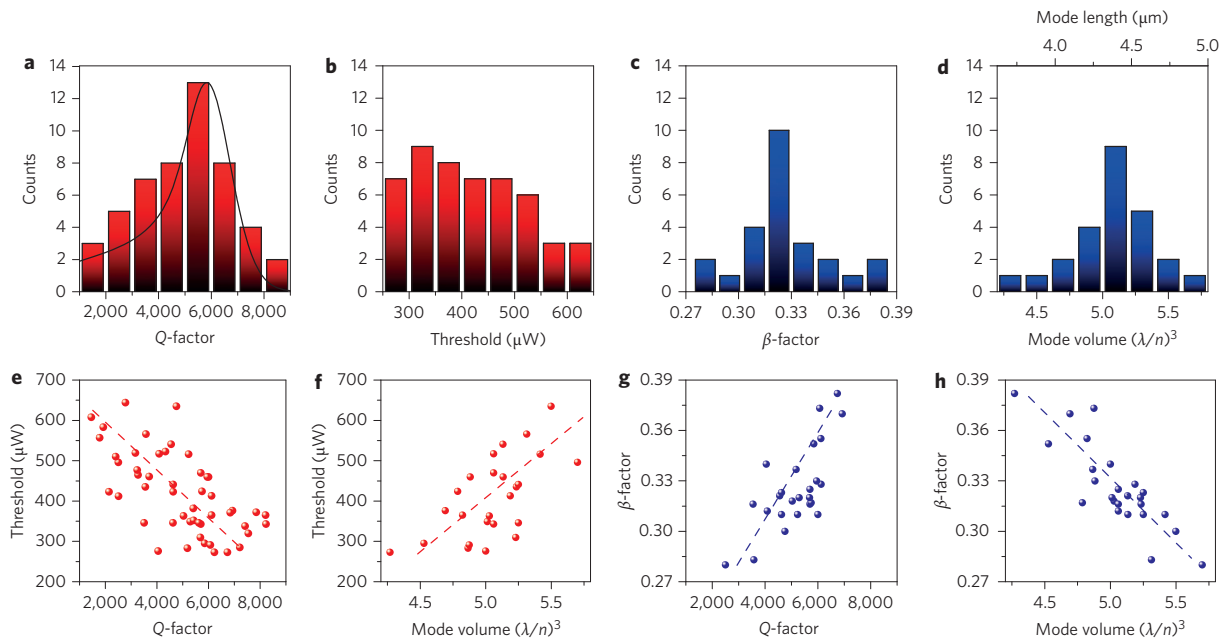


**Figure 3 | Statistical properties of random lasing in the Anderson localization regime.** **a**, Experimental Q-factor distribution of the observed localized modes in the photonic-crystal waveguide at threshold power (histograms) fitted with a one-dimensional multiple-scattering model to extract the localization length (black line). **b**, Laser-threshold distribution obtained from measured input-output curves. **c,d**,  $\beta$ -factor (**c**) and mode volume (**d**, converted to mode length on the top axis) distributions extracted from measured input-output curves. **e-h**, Measured threshold (**e,f**) and  $\beta$ -factor (**g,h**) versus Q-factor and mode volume. The Spearman's rank correlation coefficients are  $r_s = -0.63$  (**e**),  $0.61$  (**f**),  $0.63$  (**g**) and  $-0.80$  (**h**), and describe the correlation of the different parameters, with 1 corresponding to perfect correlation and  $-1$  to perfect anticorrelation. Dashed lines are guides to the eye.

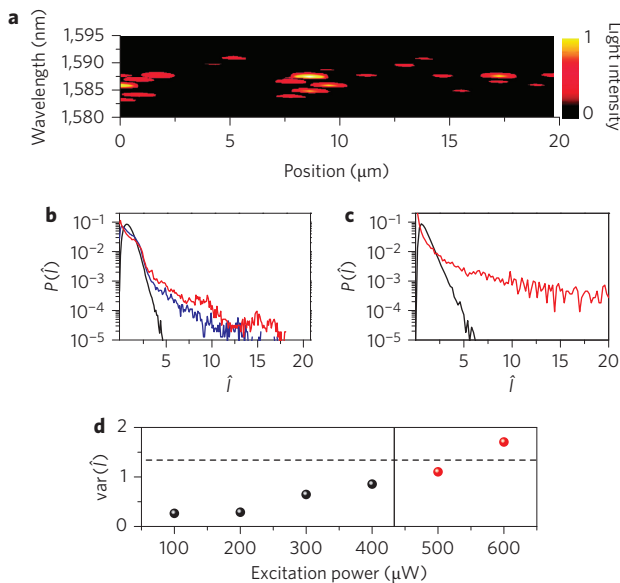


**Figure 4 | Intensity fluctuations in the Anderson localized regime.** **a**, Photoluminescence intensity for an excitation power of  $500 \mu\text{W}$  collected while scanning the excitation and collection objective along a photonic-crystal waveguide. **b**, Intensity probability distribution for excitation powers of  $100 \mu\text{W}$  (black curve),  $400 \mu\text{W}$  (blue) and  $600 \mu\text{W}$  (red). **c**, Calculated intensity probability distribution with the model of ref. 24 with a localization length of  $\xi = 6 \mu\text{m}$  and a loss length of  $l = 8 \mu\text{m}$  (black) and  $l = 800 \mu\text{m}$  (red), which corresponds to the loss length extracted from the Q-factor distributions measured at threshold. **d**, Variance of the normalized intensity as a function of excitation power. The horizontal dashed line shows the localization criterion of  $\text{var}(\hat{I}) = 1.37$ , and the vertical line indicates the excitation power corresponding to the average lasing threshold. Random lasing occurs above this threshold (red points).

Embedding light emitters in Anderson localized random media provides a promising new route to an enhanced light-matter interaction relying on the natural occurrence of cavities in random media rather than nano-engineering. This rich and intricate physics is currently being explored. The potential applications of low-threshold nanolasers and highly efficient single-photon sources are very attractive because the relevant figures of merit for these applications match engineered systems, with the added value that random structures could be much easier to fabricate. The fundamental limits of the disordered media are yet to be explored, but their performance is likely to be improved even further by deliberately mixing the amount of order and disorder in the structures. An important issue for applications of an Anderson localized nanolaser will be the ability to couple light from the randomly positioned laser to a well-defined single mode. This could easily be implemented on-chip by positioning another photonic-crystal waveguide, tailored to the non-localizing 'fast-light' regime, next to the Anderson localizing waveguide, which would enable a highly efficient and stable multi-colour random laser with directional output.

## Methods

The semiconductor heterostructure used for the fabrication of the photonic-crystal waveguides was grown on a (100)-oriented semi-insulating InP substrate by metal-organic chemical vapour deposition. The structure consisted of a 340-nm-thick  $\text{In}_{0.77}\text{GaAs}_{0.503}\text{P}$  membrane, grown on a 100-nm-thick InP, 100-nm-thick InAlAs and 800-nm-thick InP sacrificial layer, incorporating ten layers of  $\text{In}_{0.75}\text{GaAs}_{0.86}\text{P}$  quantum wells at the centre with a thickness of 5 nm and a separation of 5 nm between adjacent quantum wells. The total refractive index of the structure was  $n = 3.4$ . The photonic-crystal waveguides were fabricated by electron-beam lithography using an electron-beam writer (JEOL JBX-9300 FS), reactive-ion etching and wet etching using HCl and HF acid solutions. Samples with a lattice constant of  $a = 380 \text{ nm}$  and a range of different hole radii ( $0.237a < r < 0.263a$ ) were fabricated. Finally, 340-nm-thick suspended membranes were formed by removing the sacrificial layer.

Microphotoluminescence measurements were carried out at room temperature. A 120 fs pulsed Ti:sapphire laser operated at 800 nm with a repetition rate of 80 MHz was used for optical pumping. An excitation beam was focused to a spot

with a diameter of 1.5  $\mu\text{m}$  on the surface of the sample using a  $\times 50$  microscope objective lens (numerical aperture of 0.65), and aligned to the photonic-crystal waveguides using piezoelectric nanopositioners. The photoluminescence signal was collected by the same objective lens within a diffraction-limited region in a wide wavelength range of  $1,500 \text{ nm} < \lambda < 1,600 \text{ nm}$ , dispersed by a 300 mm grating spectrograph with a spectral resolution of 0.1 nm, and detected using a liquid-nitrogen-cooled InGaAs charge-coupled device camera.

We measured a total of 25 input–output curves by varying the excitation and collection position along the photonic-crystal waveguide. The laser threshold was obtained by extrapolating each input–output curve in a linear scale to zero power. The  $Q$ -factor was extracted by fitting the cavity mode with a Lorentzian at the threshold power. Two of the 25 input–output curves also show the cavity mode below laser threshold (Fig. 1b shows one example). For the rest of the measurements, the excitation power at which the cavity mode appeared matched the threshold power extracted from the input–output curve fitting. Based on this fact, we could increase the statistics of threshold and  $Q$ -factor distributions by gradually increasing the excitation power and recording the power at which the mode appears and its corresponding spectrum. By doing so, 25 extra data points for the laser threshold and  $Q$ -factor were added without recording the full input–output curve. The full data set is plotted in Fig. 3c,d.

The intensity probability distribution  $P(\hat{I})$  was measured by collecting the intensity  $I_{x,y}^A$ , while scanning the excitation and collection objective along a photonic-crystal waveguide with  $r/a = 0.24$  at each spatial position  $(x, y)$  with a spatial binning size of 0.25  $\mu\text{m}$  and at different wavelengths with a binning size of 1 nm. Subsequently, an average over the wavelength range 1,580–1,595 nm was performed.

Received 6 November 2013; accepted 31 January 2014;  
published online 23 March 2014

## References

- Baba, T. Slow light in photonic crystals. *Nature Photon.* **2**, 465–473 (2008).
- O'Brien, J. L., Furusawa, A. & Vučković, J. Photonic quantum technologies. *Nature Photon.* **3**, 687–695 (2009).
- Chang, D. E., Sørensen, A. S., Hemmer, P. R. & Lukin, M. D. Quantum optics with surface plasmons. *Phys. Rev. Lett.* **97**, 053002 (2006).
- Strauf, S. & Jahnke, F. Single quantum dot nanolaser. *Laser Photon. Rev.* **5**, 607–633 (2011).
- Noda, S. Seeking the ultimate nanolaser. *Science* **314**, 260–261 (2006).
- Sapienza, L. *et al.* Cavity quantum electrodynamics with Anderson localized modes. *Science* **327**, 1352–1355 (2010).
- Cao, H. *et al.* Random laser action in semiconductor powder. *Phys. Rev. Lett.* **82**, 2278–2281 (1999).
- van de Molen, K. L., Tjerkstra, R. W., Mosk, A. P. & Lagendijk, A. Spatial extent of random laser modes. *Phys. Rev. Lett.* **98**, 143901 (2007).
- Tureci, H. E., Ge, L., Rotter, S. & Stone, A. D. Strong interactions in multimode random lasers. *Science* **320**, 643–646 (2008).
- Gottardo, S. *et al.* Resonance-driven random lasing. *Nature Photon.* **2**, 429–432 (2008).
- Wiersma, D. S. The physics and applications of random lasers. *Nature Phys.* **4**, 359–367 (2008).
- Fallert, J. *et al.* Co-existence of strongly and weakly localized random laser modes. *Nature Photon.* **3**, 279–282 (2009).
- Leonetti, M., Conti, C. & Lopez, C. The mode-locking transition of random lasers. *Nature Photon.* **5**, 615–617 (2011).
- Mujumdar, S., Türeci, V., Torre, R. & Wiersma, D. S. Chaotic behavior of a random laser with static disorder. *Phys. Rev. A* **76**, 033807 (2007).
- Anderson, P. W. Absence of diffusion in certain random lattices. *Phys. Rev.* **109**, 1492–1505 (1958).
- Stano, R. & Jacquod, P. Suppression of interactions in multimode random lasers in the Anderson localized regime. *Nature Photon.* **7**, 66–71 (2013).
- Milner, V. & Genack, A. Z. Photon localisation laser: low-threshold lasing in a random amplifying layered medium via wave localisation. *Phys. Rev. Lett.* **94**, 073901 (2005).
- Yang, J. *et al.* Lasing in localized modes of a slow light photonic crystal waveguide. *Appl. Phys. Lett.* **98**, 241107 (2012).
- Joannopoulos, J. D., Johnson, S. G., Winn, J. N. & Meade, R. D. *Photonic Crystals: Molding the Flow of Light* (Princeton Univ. Press, 2008).
- Frank, R., Lubatsch, A. & Kroha, J. Theory of strong localisation effects of light in disordered loss or gain media. *Phys. Rev. B* **73**, 245107 (2006).
- Schwartz, T., Bartal, G., Fishman, S. & Segev, M. Transport and Anderson localisation in disordered two-dimensional photonic lattices. *Nature* **446**, 52–55 (2007).
- Gregersen, N., Suhr, T., Lorke, M. & Mørk, J. Quantum-dot nano-cavity lasers with Purcell-enhanced stimulated emission. *Appl. Phys. Lett.* **100**, 131107 (2012).
- Altug, O. & Vučković, J. Photonic crystal nanocavity array laser. *Opt. Express* **13**, 8819–8828 (2005).
- Smolka, S. *et al.* Probing the statistical properties of Anderson localisation with quantum emitters. *New J. Phys.* **13**, 063044 (2011).
- Thyresttrup, H., Smolka, S., Sapienza, L. & Lodahl, P. Statistical theory of a quantum emitter strongly coupled to Anderson localized modes. *Phys. Rev. Lett.* **108**, 113901 (2012).
- Ramy, G. S., Dardiry, E. & Lagendijk, A. Tuning random lasers by engineered absorption. *Appl. Phys. Lett.* **98**, 161106 (2011).
- Smolka, P. D., Smolka, S., Stobbe, S. & Lodahl, P. Density of states controls Anderson localisation in disordered photonic crystal waveguides. *Phys. Rev. B* **82**, 165103 (2010).
- Apalkov, V. M. & Raikh, M. E. Universal fluctuations of the random lasing threshold in a sample of a finite area. *Phys. Rev. B* **71**, 054203 (2005).
- Tulek, A., Polson, R. C. & Vardeny, Z. V. Naturally occurring resonators in random lasing of  $\pi$ -conjugated polymer films. *Nature Phys.* **6**, 303–310 (2010).
- Loncar, M., Yoshie, T., Scherer, A., Gogna, P. & Qiu, Y. Low-threshold photonic crystal laser. *Appl. Phys. Lett.* **81**, 2680–2682 (2002).
- Garcia, P. D., Stobbe, S., Soellner, I. & Lodahl, P. Nonuniversal intensity correlations in a two-dimensional Anderson localizing random medium. *Phys. Rev. Lett.* **109**, 253902 (2012).
- Grgic, J. *et al.* Fundamental limitations to gain enhancement in periodic media and waveguides. *Phys. Rev. Lett.* **108**, 183903 (2012).
- Yamilov, A. & Payne, B. Classification of regimes of wave transport in quasi-one-dimensional non-conservative random media. *J. Mod. Opt.* **57**, 1916–1921 (2010).

## Acknowledgements

The authors thank E. Semenova for epitaxial growth. The authors acknowledge financial support from the Danish Council for Independent Research (Natural Sciences and Technology and Production Sciences), the European Research Council (ERC consolidator grant) and the Villum Foundation (NATEC centre of excellence).

## Author contributions

J.L. and M.S. carried out the optical experiments. S.E. and M.S. fabricated the sample. J.L. and P.D.G. analysed the experimental data. N.G., T.S. and J.M. developed the rate equation models. J.L., P.D.G., S.S. and P.L. wrote the manuscript. J.M., S.S. and P.L. supervised the project. All authors read and commented on the manuscript.

## Additional information

Supplementary information is available in the online version of the paper. Reprints and permissions information is available online at [www.nature.com/reprints](http://www.nature.com/reprints). Correspondence and requests for materials should be addressed to P.L.

## Competing financial interests

The authors declare no competing financial interests.